Synchronized populations resist persistent infection

Kanishk Jain

A dissertation submitted for the partial fulfilment of BS-MS dual degree in Science

Indian Institute of Science Education and Research Mohali
April 2017

Certificate of Examination

This is to certify that the dissertation titled **Synchronized populations resist persistent infection** submitted by **Kanishk Jain** (Reg. No. MS12009) for the partial fulfillment of BS-MS dual degree programme of the Institute, has been examined by the thesis committee duly appointed by the Institute. The committee finds the work done by the candidate satisfactory and recommends that the report be accepted.

Dr. Kamal P. Singh Dr. Abhishek Chaudhuri Dr. Sudeshna Sinha
(Supervisor)

Dated: April 20, 2017

Declaration

The work presented in this dissertation has been carried out by me under the guidance of Dr. Sudeshna Sinha at the Indian Institute of Science Education and Research Mohali.

This work has not been submitted in part or in full for a degree, a diploma, or a fellowship to any other university or institute. Whenever contributions of others are involved, every effort is made to indicate this clearly, with due acknowledgement of collaborative research and discussions. This thesis is a bonafide record of original work done by me and all sources listed within have been detailed in the bibliography.

Kanishk Jain
(Candidate)

Dated: April 20, 2017

In my capacity as the supervisor of the candidates project work, I certify that the above statements by the candidate are true to the best of my knowledge.

Dr. Sudeshna Sinha
(Supervisor)

Acknowledgment

First and foremost, I would like to express my deepest gratitude to my supervisor Professor Sudeshna Sinha for her unwavering support and mentorship throughout the project. I would also like to thank Promit Moitra for being a constant source of motivation and support, and other group members Pranay Rungta, Chandrakala Meena, Manaoj Aravind and Sudhanshu Chaurasia for always being accommodating and resourceful.

I also thank the thesis committee members, Dr. Kamal P. Singh and Dr. Abhishek Chaudhuri for their constructive comments, suggestions and critiquing.

I would also like to use this opportunity to thank the Department of Physics and the Central Library of IISER Mohali for the academic support and resources.

Words fall short to thank my parents and brother Hardik for all the unceasing love, care, support and encouragement, whose value to me only grows with age.

To other family members and friends, and others who in one way or another shared their moral support through times, thank you.

List of Figures

Contents

Abstract

In this thesis, we explore the emergence of persistent infection in a closed region of space. Here the disease progression of the individuals is given by the SIRS model, namely **S**usceptible-**I**nfected-**R**efractory-**S**usceptible disease cycle. An individual becomes infected on contact with another infected individual within a given neighbourhood. We focus on the role of synchronization in the persistence of contagion. Our key result is that higher degree of synchronization inhibits persistence of infection. We demonstrate this result through different order parameters, reflecting both global and local synchronization of the phases of the disease in the individuals. We consider both asymptotic as well as finite time measures of the synchronization parameters. Our analysis of the synchronization in the disease cycle of individuals in a population shows that early asynchrony in the population, both globally and at the local level appear to be a consistent precursor to future persistence of infection. This is an important indication, since it can provide valuable early warning signals for a higher degree of persistence of infection in a population, thus enabling us to take suitable early action.[1]

[1]The results in this thesis are now being prepared for publication. The manuscript for the same is in preparation.

Introduction

Studies of epidemiological models and the spatio-temporal dynamics of disease propagation has attracted considerable research attention over the years. These studies have also contributed in the development of various mathematical models that accurately describe the dynamics of infectious disease propagation[EK88, Mur93, RSBY03]. These investigations focus on the spatial dynamics of the population, particularly studying the degree and extent of the spread of infection on different population topologies, for example, on a uniform lattice, or on small-world networks, as well as the temporal dynamics of these disease models, where the model parameters quantify the transfer rate of infection between the individuals in the population. Some of these studies look at simple epidemiology models where the infection is fatal, and the susceptibility and the transmissibility of infection through local neighbours is probabilistic on a small-world network[MN00]. Other models consider the case where individuals attain a permanent immunity after a temporary infection period. There is no prevalence of infection in such cases as the susceptible population slowly decreases with time[ML01]. Others have probed further and studied models with a temporary immune period, following which an individual is susceptible again[LHS08]. Studies of such models on small-world networks have shown an increase in persistence of infection when the number of random connections are sufficiently large[KA01]. Other studies on time-varying networks show frequent epidemic outbreaks as compared to static networks[KS13].

A large class of studies also employ sets of differential equations[Het76] or difference equations[GCNS02] to model disease propagation. Such models are relevant for homogeneous well-mixed populations, where infection arises from random encounters of individuals and spatial structure in populations is disregarded.

In this thesis we will consider a cellular automata model of disease propagation on a 2-d lattice with probabilistic infection rules and deterministic disease cycles.

We will consider heterogeneous systems and try to correlate features of the initial time evolution of the system with asymptotic persistence of infection. We start by describing the model for disease progression below and go on to describe the condition of infection.

The SIRS Disease Cycle

In this study, we explore the SIRS disease cycle which has four compartments: susceptible(**S**), Infected(**I**) or Refractory(**R**). An individual can be in either of these state during the disease cycle. Upon infection, the individual goes through the infected stage of the disease. This is followed by the temporarily immune stage, known as the refractory stage of the disease cycle. After the refractory phase the individual is susceptible to infection again, and returns to the susceptible state . This is shown schematically in Fig. 1.

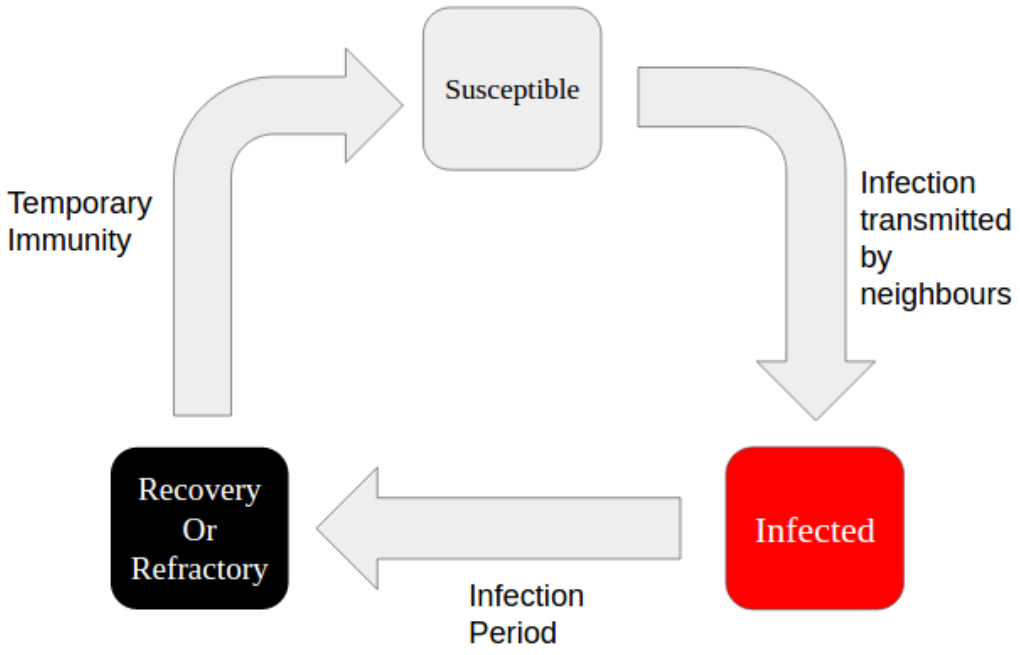

Figure 1: The SIRS disease cycle. A susceptible individual gets infected after coming in contact with an infected neighbour, then susbesquently moving to the refractory stage where it is temporarily immune to the infection.

Mathematical model describing the disease cycle: We consider a cellular automata model of disease progression, where time t evolves in discrete steps, with each individual, indexed by (i, j) on a 2 dimensional lattice, characterized by a counter

$$\tau_{i,j}(t) = 0, 1, \ldots, \tau_I + \tau_R$$

describing its *phase* in the cycle of the disease [AMS17]. Here $\tau_I + \tau_R = \tau_0$, where τ_0 signifies the total length of the disease cycle. At any instant of time t, if phase $\tau_{i,j}(\mathrm{t}) = 0$, then the individual at site (i, j) is susceptible; if $1 \leq \tau_{i,j}(t) \leq \tau_I$, then it is infected; if phase $\tau_{i,j}(t) > \tau_I$, it is in the refractory stage. For, phase $\tau_{i,j}(t) \neq 0$ the dynamics is given by the counter updating by 1 every time step, and at the end of the refractory period the individual becomes susceptible again, i.e. if $\tau_{i,j}(t) = \tau_0$ then, $\tau_{i,j}(t + 1) = 0$. Namely:

$$\begin{aligned} \tau_{i,j}(t+1) &= \tau_{i,j}(t) + 1 \qquad \text{if } 1 \leq \tau_{i,j}(t) < \tau_0 \quad (1) \\ &= 0 \qquad\qquad\quad \text{if } \tau_{i,j}(t) = \tau_0 \quad (2) \end{aligned}$$

Hence the disease progression is a *cycle*. We consider the typical condition where the refractory period is longer than the infective stage, i.e. $\tau_R > \tau_I$. In our simulations, we chose to keep $\tau_I = 4$ and $\tau_R = 9$ with no loss of generality.

The initial fraction of susceptible, infected and refractory individuals in the populations are denoted by S_0, I_0 and R_0 respectively. Similarly, the fractions at time t are denoted by S_t, I_t and R_t.

Transmission of infection

Here we consider the condition that a susceptible individual (S) will become infected (I) *if one or more of its nearest neighbours are infected*. That is, if $\tau_{i,j}(t) = 0$, (namely, the individual is susceptible), then $\tau_{i,j}(t+1) = 1$, if any $1 \leq \tau_{x,y}(t) \leq \tau_I$ where x, y lies in its neighbourhood consisting of K nearest individuals. In this study we consider neighborhoods of two different sites, namely $K = 4$ and 8. The neighbourhood $K = 4$ includes the neighbours at sites $(i-1, j)$, $(i+1, j)$, $(i, j-1)$ and $(i-1, j+1)$. The neighbourhood $K = 8$ includes the neighbours in $K = 4$, and additionally includes the neighbours at sites $(i-1, j-1)$, $(i-1, j+1)$, $(i+1, j-1)$, $(i+1, j+1)$. The

transmission of infection for both the cases for illustrative examples, are shown in Fig. 2.

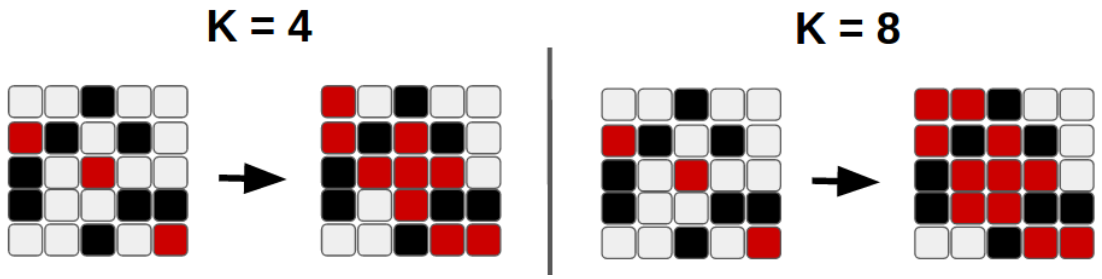

Figure 2: Transmission of infection for both $K = 4$ and $K = 8$ cases. It is clear that for $K = 4$, infection is transmitted to the individual at positions $(i-1, j)$, $(i+1, j)$, $(i, j-1)$ and $(i-1, j+1)$, whereas for $K = 8$, infection is transmitted to the individuals at $(i-1, j-1)$, $(i-1, j+1)$, $(i+1, j-1)$, $(i+1, j+1)$ as well.

Tools used to study the model

We used **Python** along with the some standard external packages for simulations and analysis. Specifically, we used *PyQt5* for simulations, and *scipy* and *matplotlib* for subsequent analysis of the simulation data.

Dynamics of disease progression in a closed population

We now study the dynamics of this SIRS disease model on a 2 dimensional square lattice. We consider a closed population where there are no individuals beyond the boundaries to either infect, or be infected by[CH84]. This is implemented by putting a fixed refractory layer along the boundaries.

We start with an initial population with the initial fraction of infected individuals $I_0 = 0.1$ while keeping the fractions of susceptible S_0 and refractory individuals R_0 equal, and satisfying the conditions $S_0 + I_0 + R_0 = 1$. A random initial condition with these parameters is shown in Fig. 3a.

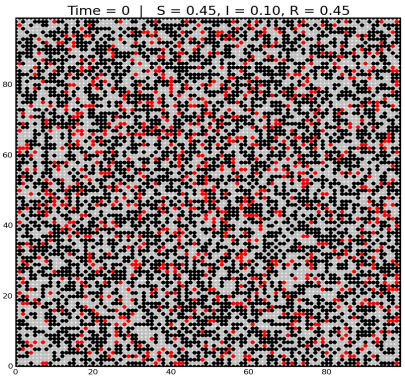

(a) Initial population at T = 0

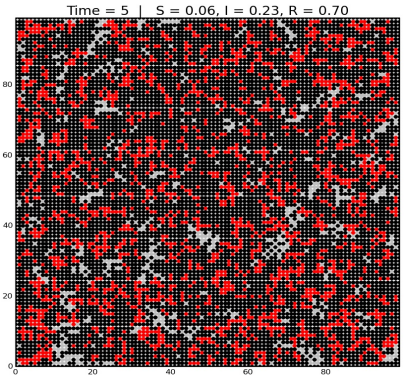

(b) T = 5

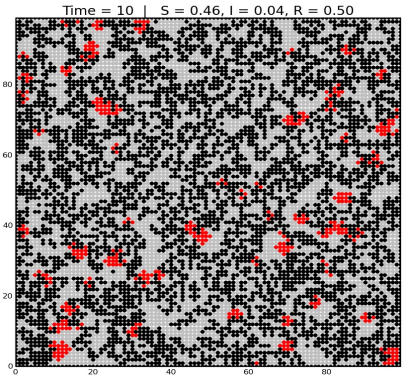

(c) T = 10

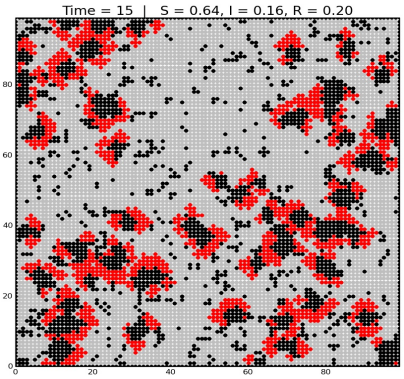

(d) T = 15

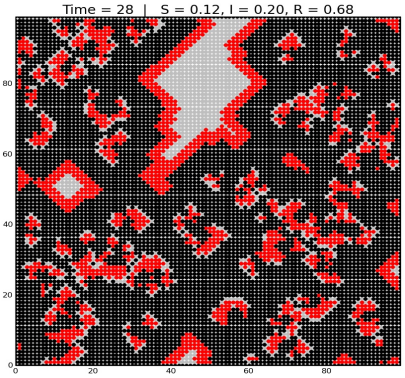

(e) T = 28

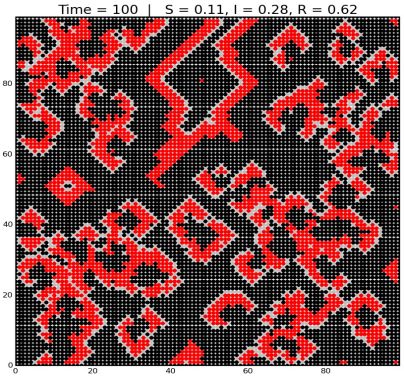

(f) T = 100

Figure 3: Snapshots at various times of a population evolving from a randomly mixed initial state with the initial fraction of infected individual $I_0 = 0.1$ and fraction of susceptible and refractory individual $S_0 = R_0 = 0.45$. The population is surrounded by a permanent refractory wall. Here, $K = 4$.

Fig. 3 shows wave like patterns emerging after some transient transitions in the population. The wave-fronts are composed of infected individuals, leaving a trail of refractory individuals behind. These waves are periodic and seem to originate from some fixed centers in the population.

Fig. 4 shows time evolution of the fraction of susceptible, infected and refractory (S, I, and R, respectively) in the population shown in Fig 3. Fig. 4 shows the trend of S, I and R with time, where the initial fractions $I_0 = 0.1$ and $S_0 = R_0 = 0.45$. After a short transient period, the fractions S_t, I_t and R_t repeat periodically over time.

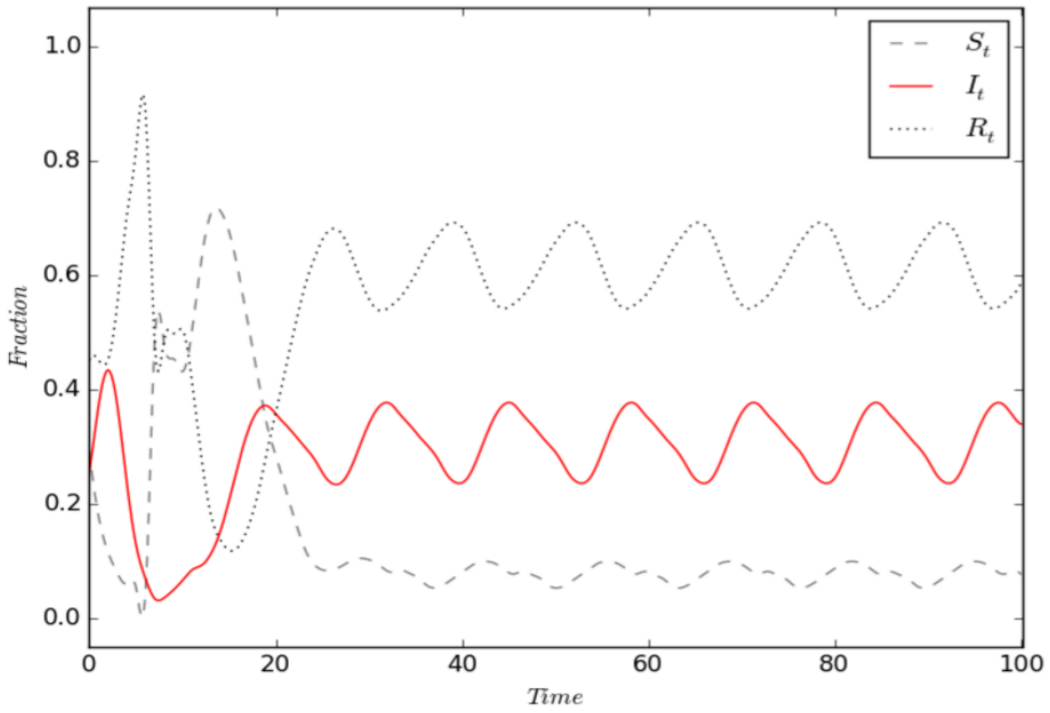

Figure 4: Time evolution of S_t, I_t and R_t in the population where $I_0 = 0.1$ and $S_0 = R_0 = 0.45$.

Results

Persistence Order Parameter

To quantify the degree of persistence in the population, we calculate the average value of the fraction of infected individuals I at asymptotic times and denote this time averaged quantity as the *Persistence Order Parameter* $\langle I \rangle$. That is

$$\langle I \rangle = |\frac{1}{T}\Sigma^T I_t| \tag{3}$$

where T is the length of the time after transience over which the quantity is averaged. $\langle I \rangle$ is nonzero when there is a non-zero fraction of infected individuals in the population at asypmtotic times and 0 otherwise.

In Fig. 5, we explore the distribution of $\langle I \rangle$ for different initial infected fraction I_0, while keeping $S_0 = R_0$. We look at this distribution for 500 different random initial conditions for each I_0 fraction, when $K = 4$ (in blue), as well as when $K = 8$ (in red). Fig. 5 counter-intuitively shows that an increase in the initial fraction of infecteds I_0 leads to the extinction of infection in a large fraction of populations. This transition to extinction of infection with increasing I_0 is quicker for $K = 8$.

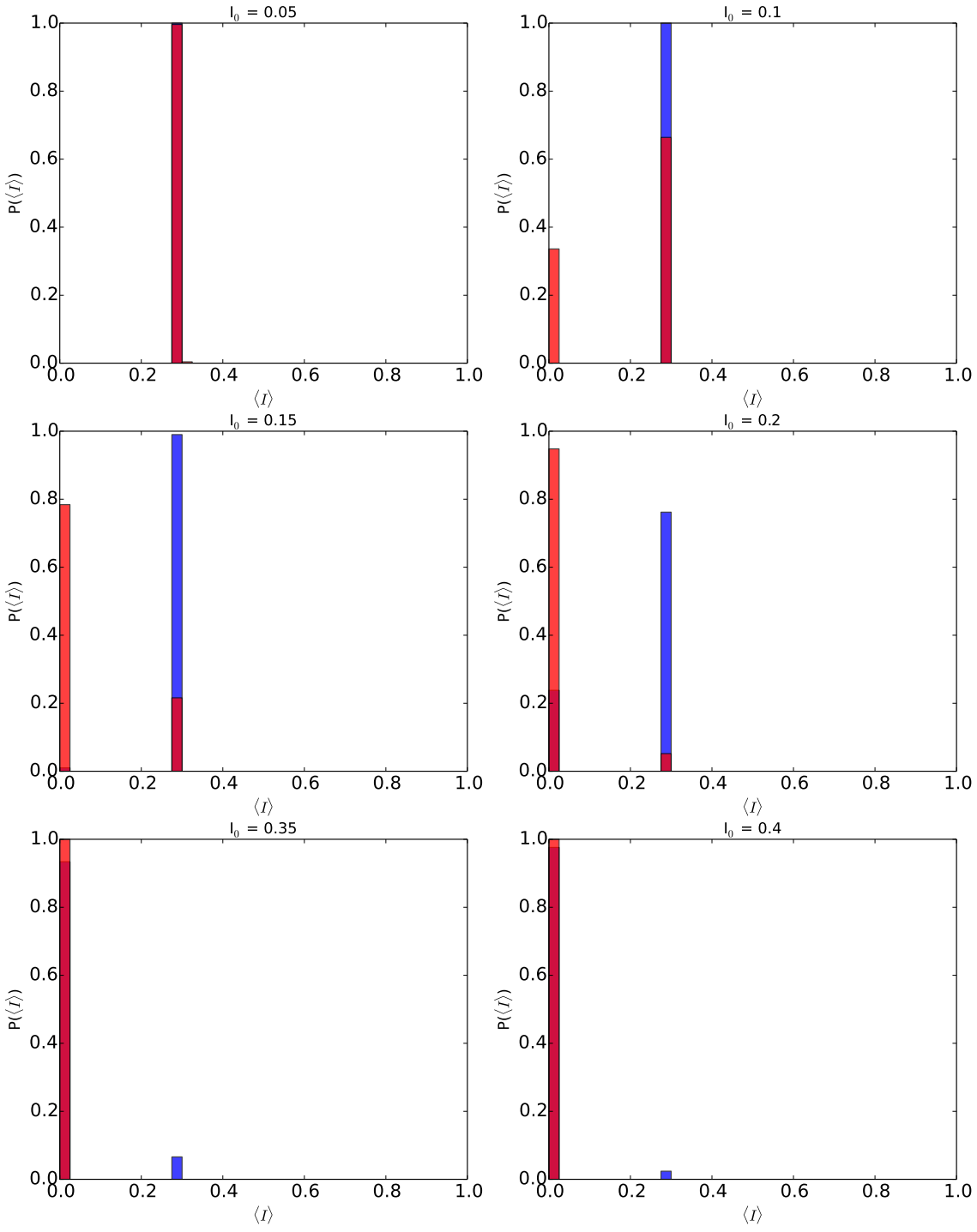

Figure 5: Distribution of the *Persistence Order Parameter* $\langle I \rangle$ for different initial fractions of infected individuals I_0 in the population. We explore this distribution for both $K = 4$ (blue) and $K = 8$ (red) cases. There is an increasing shift to extinction of infection in the population as I_0 increases, the shift being faster for $K = 8$ case.

Global Synchronization Order Parameter

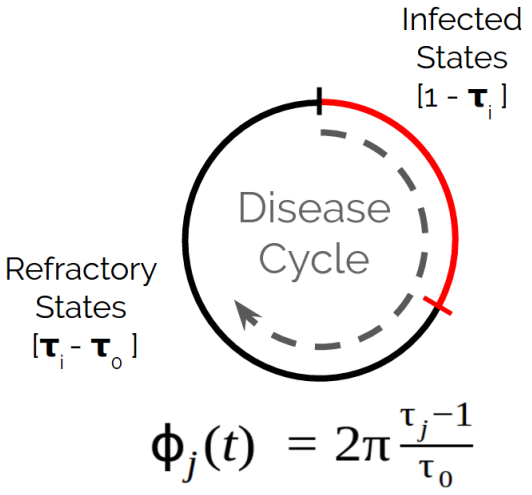

Figure 6: Illustration of the geometric phase of a disease stage in the SIRS disease cycle.

We first explore the degree of global synchronization in the system, by calculating synchronization in the population defined as,

$$\sigma(t) = |\frac{1}{N}\Sigma^{N} \exp^{i\phi_{m,n}(t)}| \tag{4}$$

where $\phi_{m,n} = 2\pi(\tau_{m,n} - 1)/\tau_0$ is a geometrical phase corresponding to the disease stage $\tau_{m,n}$ of the individual at site (m, n), as shown in Fig. 6. Here the indices m and n run over the N infected and refractory individuals in the population. We chose to include only infected and refractory individuals in this calculation as they contribute to the deterministic dynamics of the model[GS05].

$\sigma(t)$ will be closer to 1 if all the individual states in the population are closer to each other in the disease cycle. To gain a clear understanding of the synchronization in different populations, we take a look at its time evolution for populations with different initial fraction of infecteds I_0. As evident from Fig. 7, the value of $\sigma(t)$ asymptotically stabilizes to small oscillations about a charachteristic value. For $I_0 = 0.3$, its value reaches 1, which signifies complete synchrony in the asymptotic population.

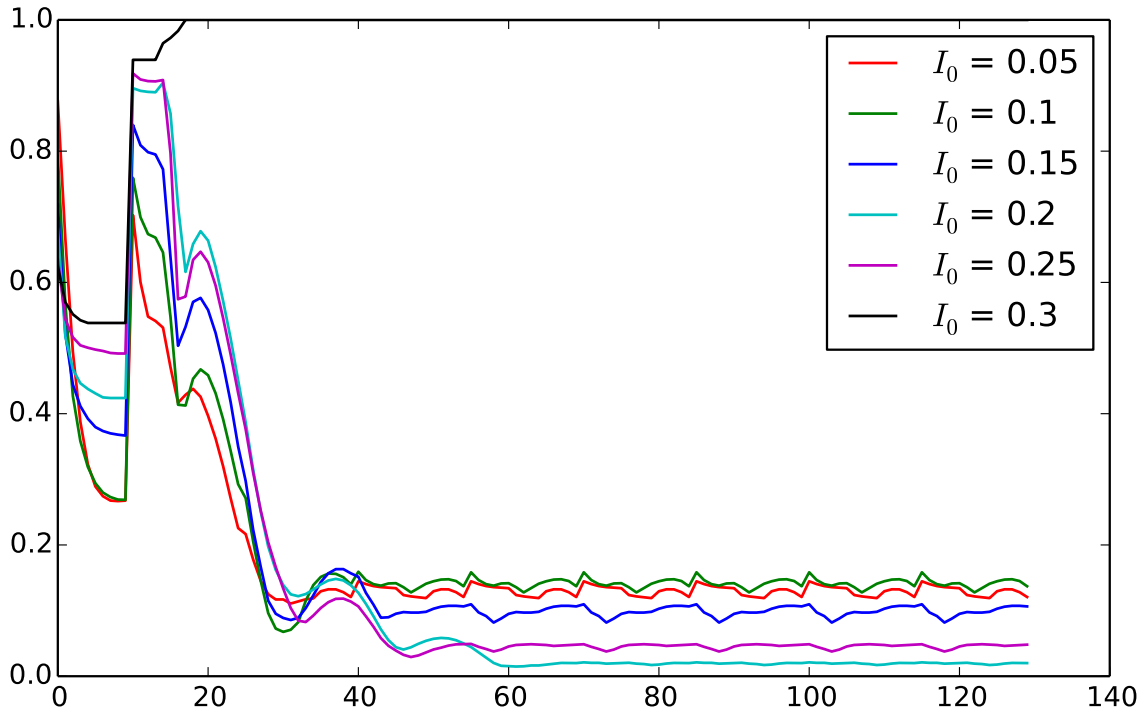

Figure 7: Time evolution of the synchronization in the population $\sigma(t)$ for different initial fraction of infected individuals. The value of $\sigma(t)$ stabilizes after some transient time. Lower values of $\sigma(t)$ signify larger degree of asynchrony in the population.

We further define the global synchronization order parameter in the population by looking at the asymptotic time averaged value of synchronization $\sigma(t)$ in the population. That is,

$$\langle \sigma \rangle = |\frac{1}{T}\Sigma^T \sigma(t)| \tag{5}$$

We look at the distribution of $\langle \sigma \rangle$ for different fractions of initially infected individuals, similar to the study done for the persistence order parameter $\langle I \rangle$. Fig. 8 shows the distribution of $\langle \sigma \rangle$ for 500 random initial conditions for different values of I_0. There is an increase in the fraction of synchronized populations at asymptotic times as we increase I_0. This shift from asynchrony to complete synchrony is faster for the case when $K = 8$.

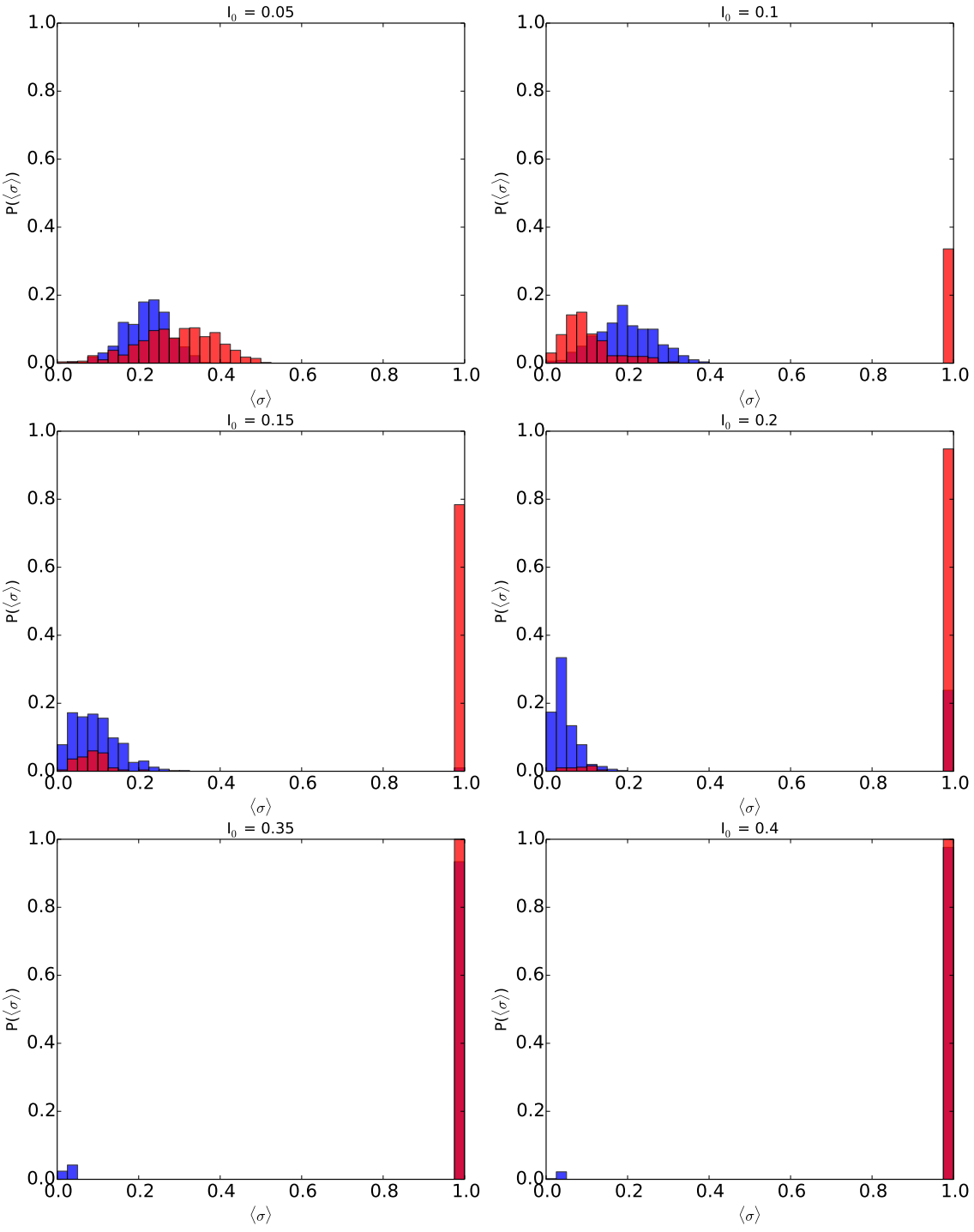

Figure 8: Distribution of the synchronization order parameter $\langle\sigma\rangle$ for population with random initial conditions for different I_0. We look at the distribution for both the cases $K = 4$ and $K = 8$.

Correlation between global synchronization and persistence

Fig. 5 shows us a difference in the distribution of the asymptotic values of the persistence order parameter $\langle I \rangle$ for different values of the initial fraction of infecteds I_0. In Fig. 9 below, we look at the ensemble averaged value of $\langle I \rangle$, and we denote this quantity as $\langle\langle I \rangle\rangle$. We calculate this quantity for different values of I_0 ranging from 0 to 1, averaged over 500 random initial conditions for each I_0. The dependence of $\langle\langle I \rangle\rangle$ on I_0 for $K = 4$ and $K = 8$ is shown in Fig. 9. *Interestingly, it indicates that the typical persistence of disease to be expected for the case of larger infective neighbourhoods, is smaller.*

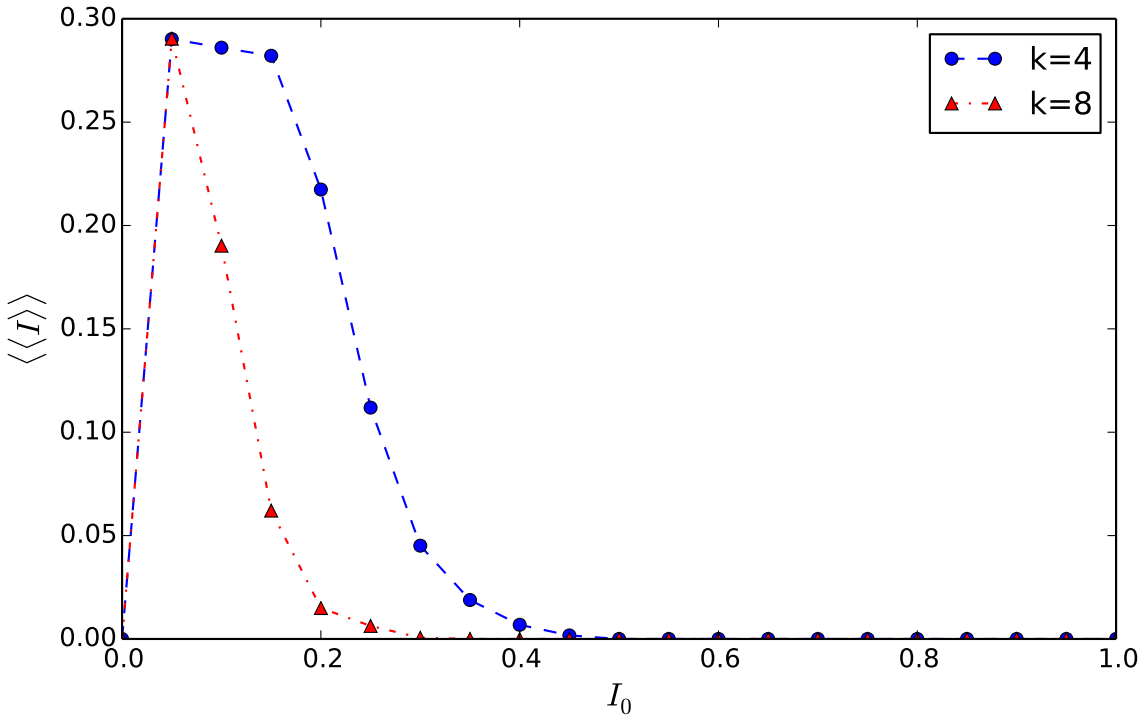

Figure 9: Dependence of the ensemble averaged persistence order parameter $\langle\langle I \rangle\rangle$ on the initial fraction of infected individual I_0, for $K = 4$ and $K = 8$. The window of persistence, i.e, the range of values of I_0 with a non-zero value of $\langle\langle I \rangle\rangle$ is smaller for $K = 8$ case.

Now, we look at the dependence of the synchronization order parameter on different values of I_0. We average the synchronization order parameter over 500 random initial conditions for each I_0 and denote this quantity as $\langle\langle \sigma \rangle\rangle$. Fig 10 shows the value of $\langle\langle \sigma \rangle\rangle$ for different values of I_0.

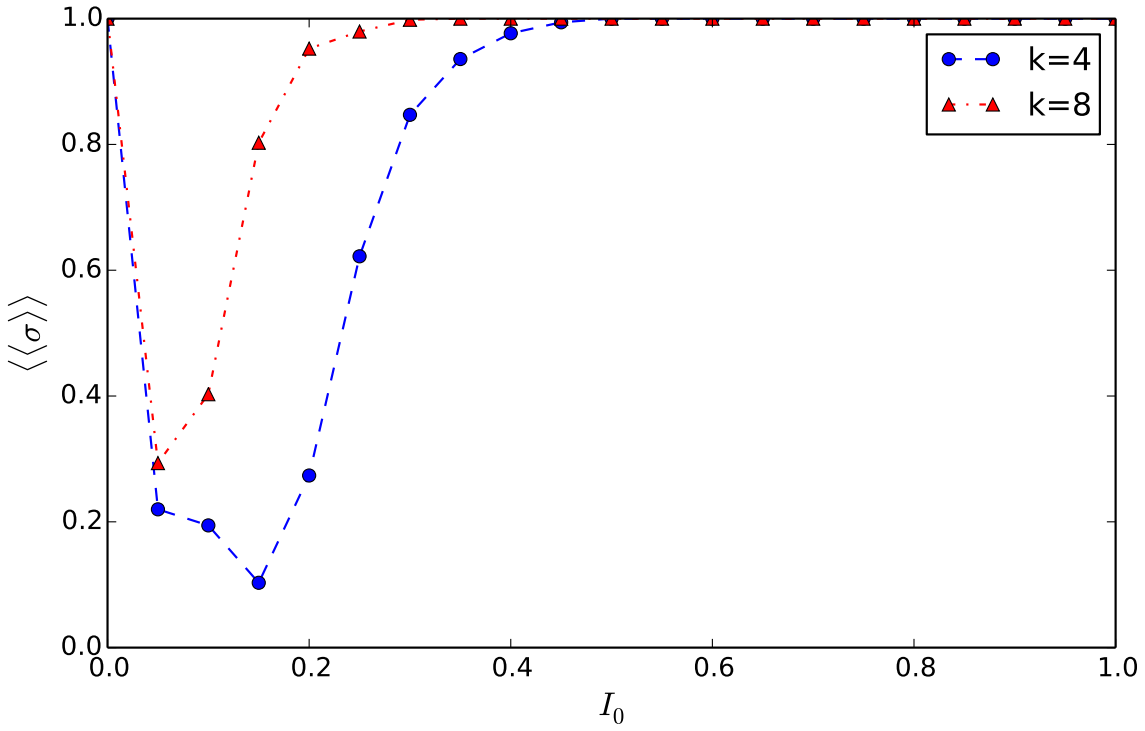

Figure 10: Dependence of the ensemble averaged synchronization order parameter $\langle\langle\sigma\rangle\rangle$ on the initial fraction of infected individuals I_0,for $K = 4$ and $K = 8$.

We now correlate the values of the persistence order parameter $\langle\langle I\rangle\rangle$ and the synchronization order parameter $\langle\langle\sigma\rangle\rangle$ obtained for different I_0, as shown in Fig. 9 and Fig. 10 above. Fig. 11 shows the correlation between $\langle\langle I\rangle\rangle$ and $\langle\langle\sigma\rangle\rangle$ for populations with $K = 4$ and $K = 8$. *It is evident from Fig. 11 that populations with a large value of synchronization order parameter have a weaker degree of final persistence in the population.*

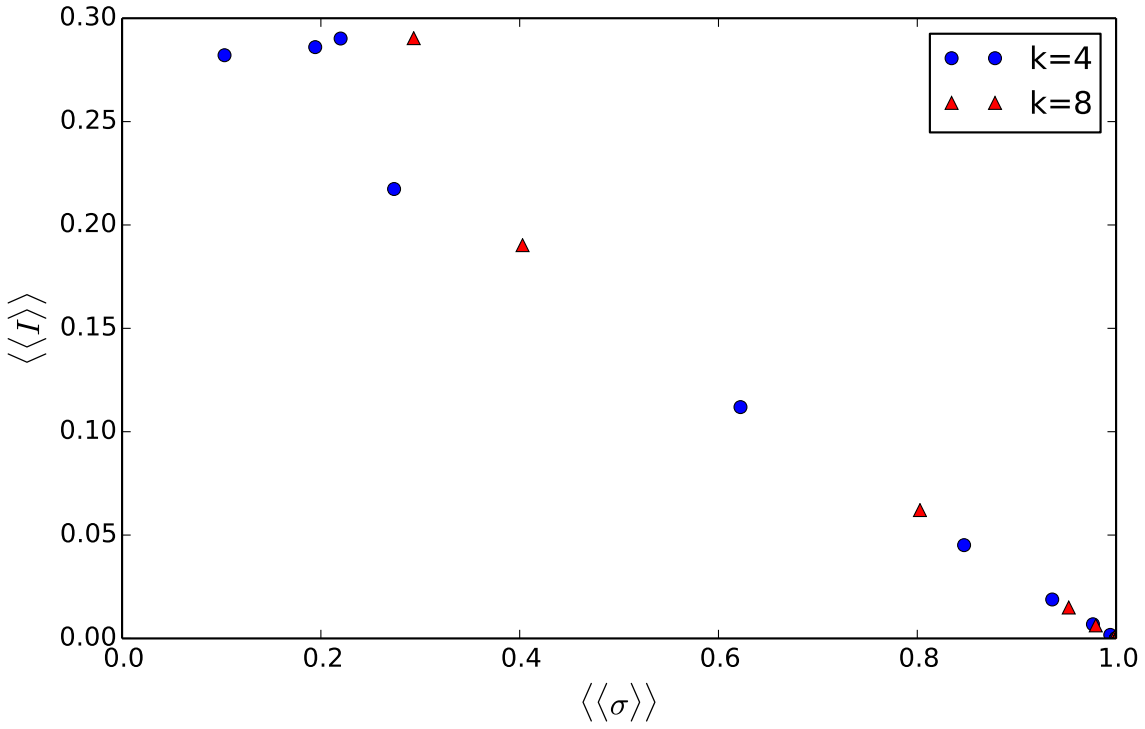

Figure 11: Correlation between $\langle\langle I \rangle\rangle$ and $\langle\langle \sigma \rangle\rangle$ for $K = 4$ and $K = 8$. In both the cases, there is a monotonic decrease in the persistence order parameter as the synchronization order parameter increases.

Local Synchronization Order Parameter

Now we explore *local synchronization*, namely synchronization in the local neighbourhood of an individual. This is important, as infection spread is a local contact process and so the composition of its local neighbourhood is most crucial for an individual. In order to capture local synchrony, we introduce a measure of local synchronization, define as:

$$\sigma_L^{(i,j)}(t) = |\frac{1}{N_{nbr}} \Sigma_{NN} \exp^{i\phi_{m,n}(t)}| \tag{6}$$

where $\phi_{m,n} = 2\pi(\tau_{m,n} - 1)/\tau_0$ is a geometrical phase corresponding to the disease stage $\tau_{m,n}$ of the individual at site (m, n). Here the indices m and n run over all infected and refractory individuals in the K neighbourhood of the individual, namely all neighbours of the individual at site (i, j). When the range of influence of an infected individual includes only the four nearest neighbours(Fig. 12), we have $K = 4$ and the sum runs over the 4 neighbouring sites.

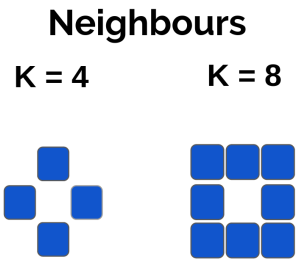

Figure 12: $K = 4$ and $K = 8$ neighbourshoods of the individuals.

In Fig. 13 and Fig. 14, we look at the distribution of $\sigma_L^{(i,j)}$ at different time windows, in 10 random initial conditions for a fixed I_0. Specifically, we are looking at the distribution of $\sigma_L^{(i,j)}(t)$ calculated for all the sites in the population during the first 15 time steps of evolution. As evident from Fig. 13, the distribution of transient local synchronization is similar for different I_0 values. The neighbourhoods of a small fraction of the sites seem to be in perfect synchrony during transience for all the initial conditions. On the other hand, the distribution of $\sigma_L^{(i,j)}(t)$ for each individual during the asymptotic times is shown in Fig. 14. Here, a sharp difference in the distribution of $\sigma_L^{(i,j)}(t)$ for differnt I_0 is evident, with a very small number of neighbourhoods synchronized for $I_0 = 0.05$ and $I_0 = 0.1$, and a large fraction of the sites with $\sigma_L^{(i,j)}(t) = 1$ for $I_0 = 0.2$. For I_0, all the neighbourhoods in the population are perfectly synchronized.

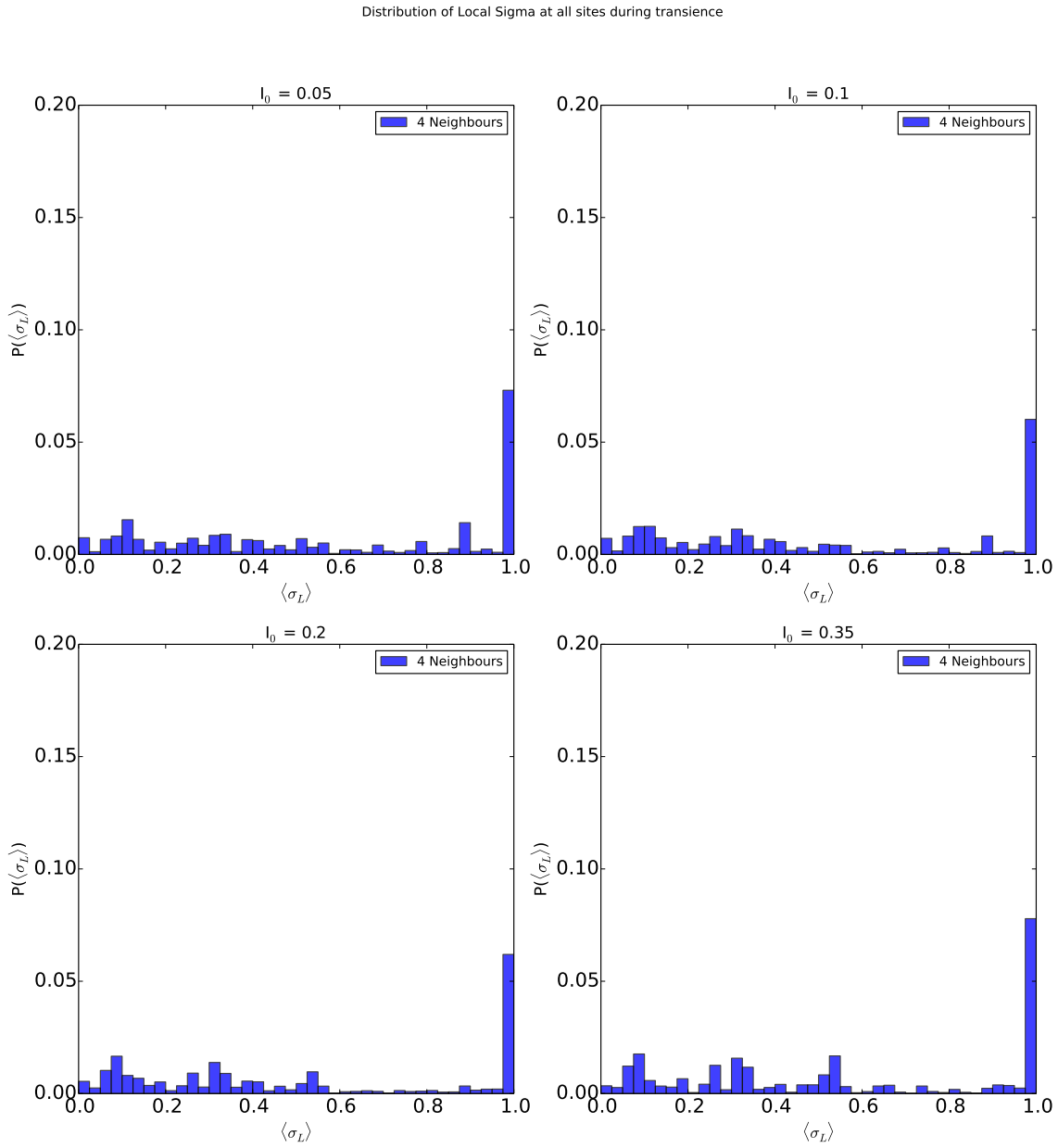

Figure 13: Distribution of the local synchronization in the population during the first 15 time steps, for different values of I_0. The distributions shown are for 10 random initial conditions for each I_0.

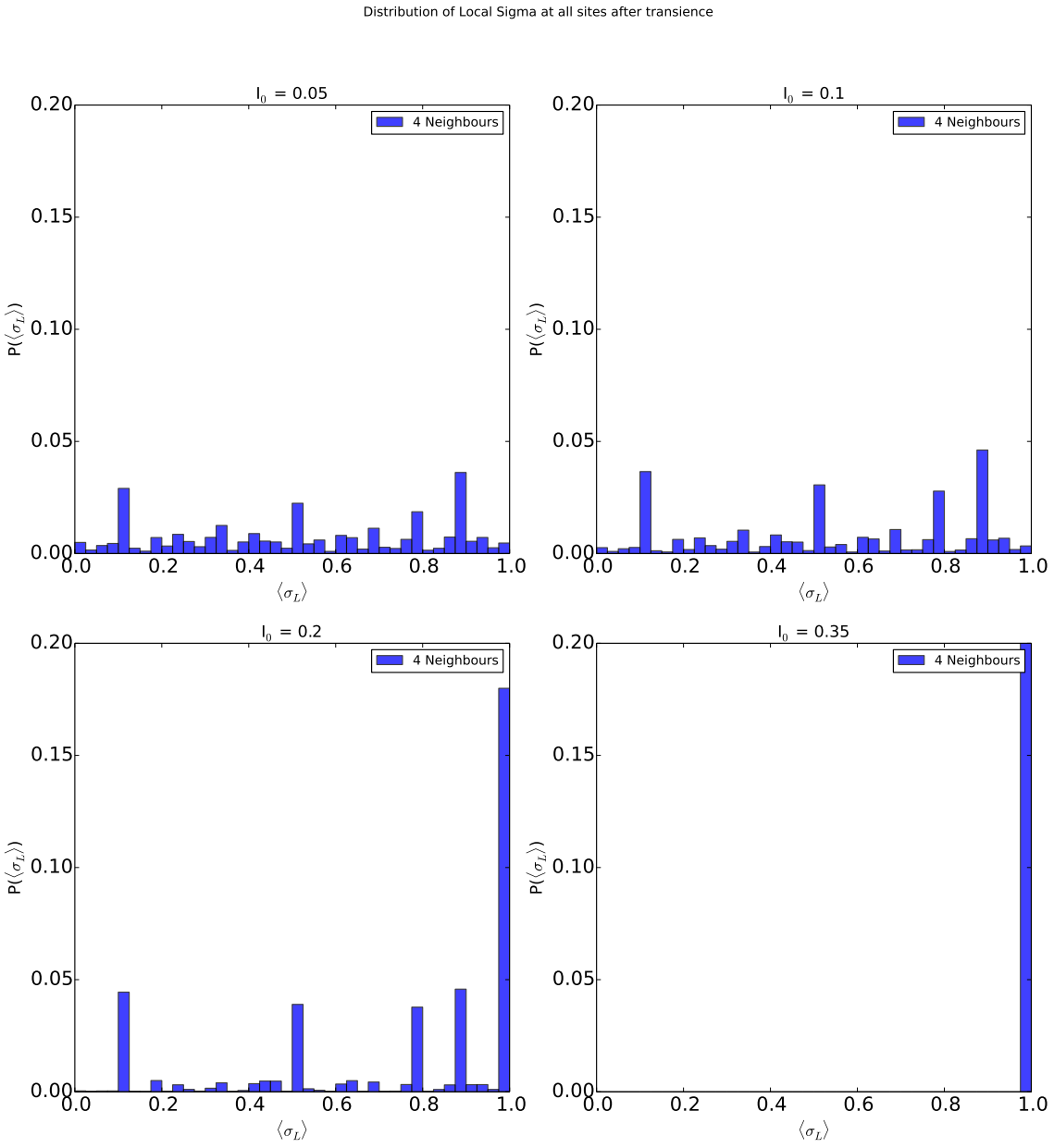

Figure 14: Distribution of the local synchronization in the population at asymptotic times, for different values of I_0. The distributions shown are for 10 random initial conditions for each I_0.

We now calculate $\sigma_L^{(i,j)}(t)$ averaged over the full lattice $1 \leq$ (i, j) $\leq$ N. This quantity reflects the *average local synchronization* in the population and is denoted by $\sigma_L(t)$. That is,

$$\sigma_L(t) = |\frac{1}{N}\Sigma^N \sigma_L^{(i,j)}(t)| \tag{7}$$

We also calculate the *Root-Mean-square Deviation* of the local synchronization (RMSD($\sigma_L(t)$)) in the population as follows,

$$RMSD(\sigma_L(t)) = \sqrt{\frac{1}{N}\Sigma^N(\sigma_L(t) - \sigma_L^{(i,j)}(t))^2} \tag{8}$$

where the index (i,j) run over all the N individuals in the population.

Further, we will consider $\sigma_L(t)$ and $RMSD(\sigma_L(t))$ averaged over different time windows. In Fig. 15, we plot the time and ensemble averaged values of $\sigma_L(t)$ and $RMSD(\sigma_L(t))$ during the asymptotic times for different values of the initial fraction of infecteds I_0. These quantities are averaged over 30 time steps, and for 500 random initial conditions for each value of I_0. We denote these quantities as $\langle\langle\sigma_L(t)\rangle\rangle$ and $\langle\langle RMSD(\sigma_L(t))\rangle\rangle$. The figure also shows the dependence of ensemble averaged persistent order parameter $\langle\langle I\rangle\rangle$ on I_0 as it was seen in Fig. 9. Fig. 15 shows that the populations have a lower value of $\langle\langle\sigma_L(t)\rangle\rangle$ and a higher value of $\langle\langle RMSD(\sigma_L(t))\rangle\rangle$ in the window of persistence.

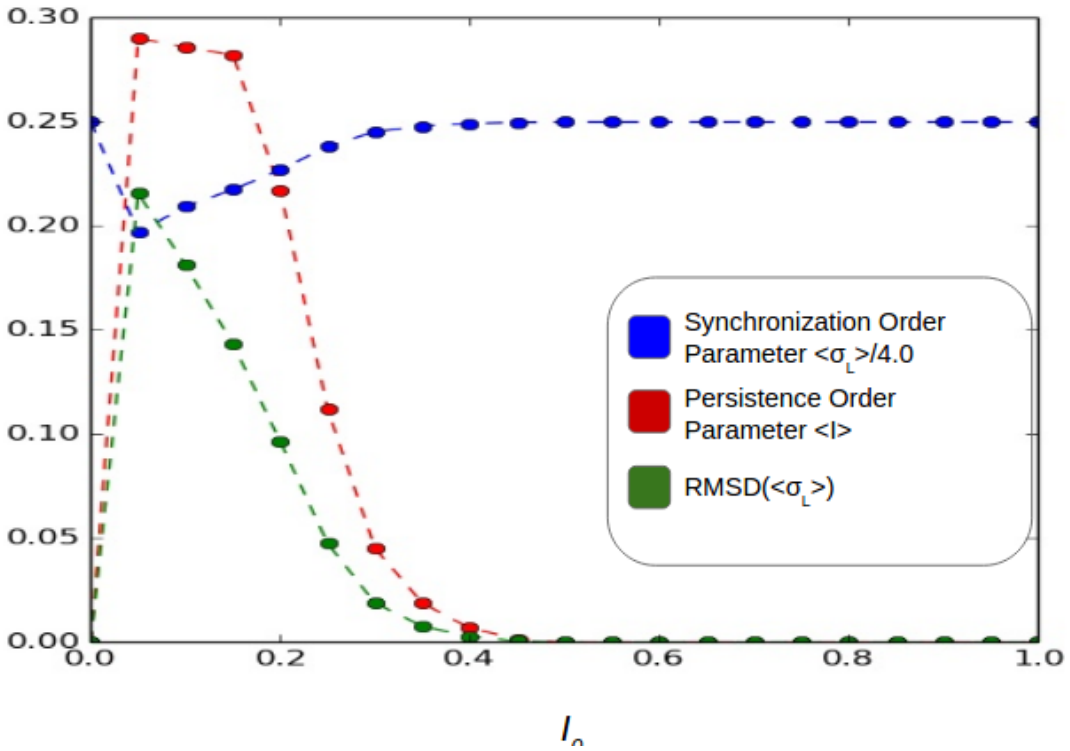

Figure 15: Dependence of the synchronization order parameter $\langle\langle\sigma_L(t)\rangle\rangle$ and the root-mean-square deviation in the local synchronization $\langle\langle RMSD(\sigma_L(t))\rangle\rangle$ on the initial fraction of infected individuals I_0 at asymptotic times. The quantities are averaged over 30 time steps after transience and for 500 different random initial conditions for each I_0, and $K = 4$.

Correlation between local synchronization and persistence

In Fig. 16 below, we correlate the asymptotic values of $\langle\langle I\rangle\rangle$ and $\langle\langle\sigma_L(t)\rangle\rangle$ obtained for different initial fraction of infecteds I_0. The figure shows that the degree of persistence in the population decreases as the value of average local synchronization of the population increases, for both $K = 4$ and $K = 8$.

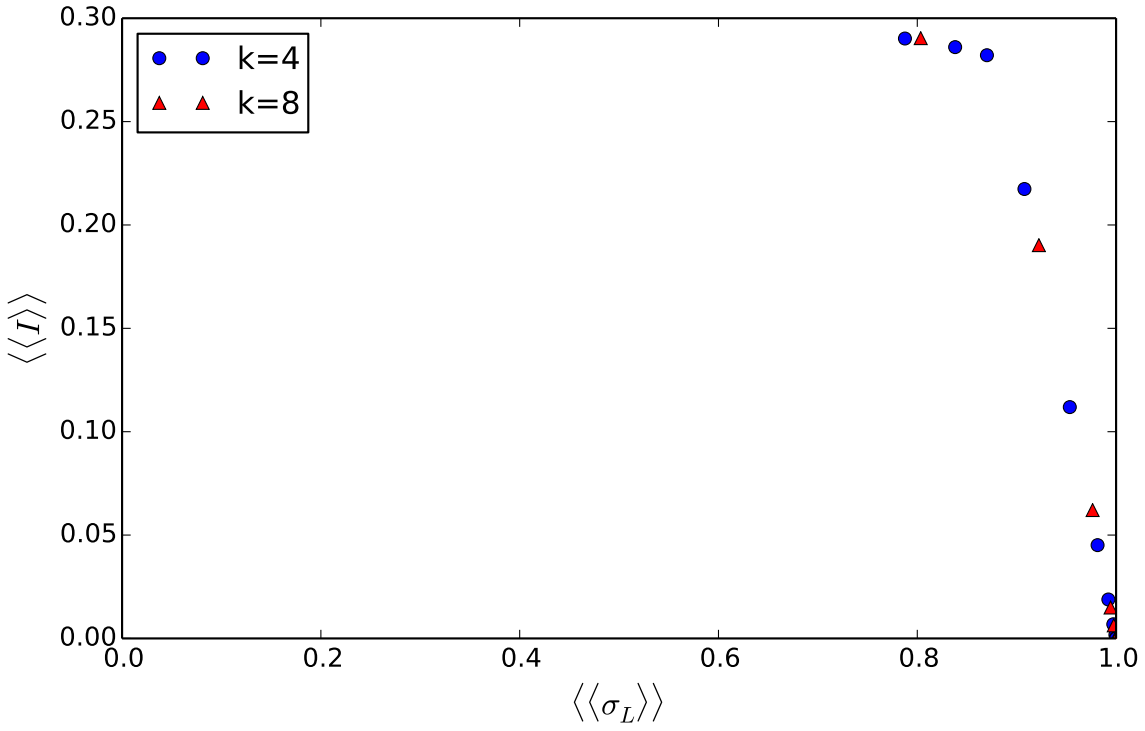

Figure 16: Correlation between the ensemble averaged persistent order parameter $\langle\langle I\rangle\rangle$ and local synchronization order parameter $\langle\langle \sigma_L(t)\rangle\rangle$ for population with different initial fraction of infected individuals I_0. The data is shown for both K= 4 and K = 8.

We also explore the correlation between persistence order parameter $\langle\langle I\rangle\rangle$ and asymptotic values of root-mean-square deviation in the local synchronization in the population $\langle\langle RMSD(\sigma_L(t))\rangle\rangle$, obtained for different initial fraction of infecteds I_0 in Fig. 17. We find that the degree of persistence in the population increases as the value of $\langle\langle RMSD(\sigma_L(t))\rangle\rangle$ increases, when $K = 4$ and $K = 8$.

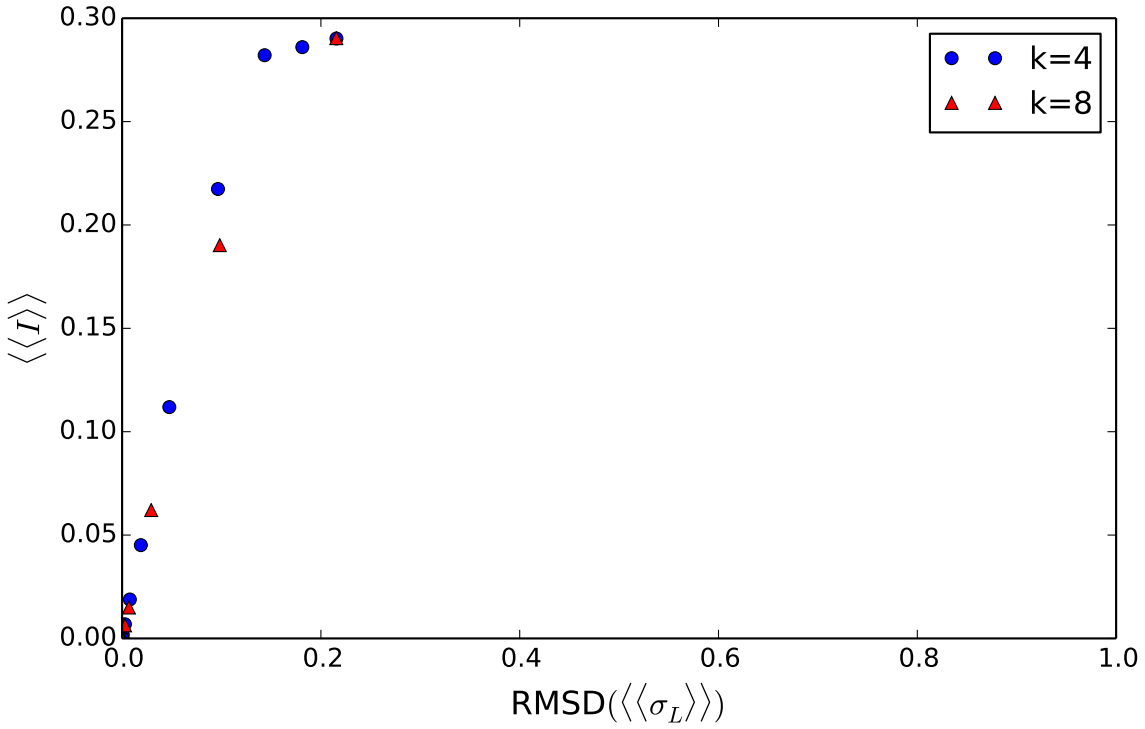

Figure 17: Correlation between the persistent order parameter $\langle\langle I \rangle\rangle$ and the root-mean-square deviation of the local synchronization in the population $\langle\langle RMSD(\sigma_L(t)) \rangle\rangle$ at asymptotic times with different initial fraction of infected individuals I_0. The figure shows data for both $K = 4$ and $K = 8$.

Transient Synchronization

In order to explore the role of transient global synchronization, we introduce a finite-time synchronization parameter, defined as:

$$\langle \sigma_T \rangle = \frac{1}{T} \Sigma_{t=0}^{T-1} \sigma(t) \tag{9}$$

where $\sigma(t)$ is given by Eqn. 4. Further we consider an ensemble-averaged value of σ_T, denoted by $\langle\langle \sigma_T \rangle\rangle$. This is obtained by averaging over a large sample of initial states with a specific I_0, S_0 and R_0. In this work we focus on $\langle \sigma_{15} \rangle$, which is the average value of the synchronization order parameter over the first 15 time steps, a period roughly equal to the first cycle of the disease.

Transient Global Synchronization

Fig. 18 shows the ensemble averaged values of $\langle\sigma_{15}\rangle$ for different initial fraction of infecteds I_0 in the population. The quantity is averaged over 500 different random initial conditions for each I_0, for $K = 4$ and $K = 8$.

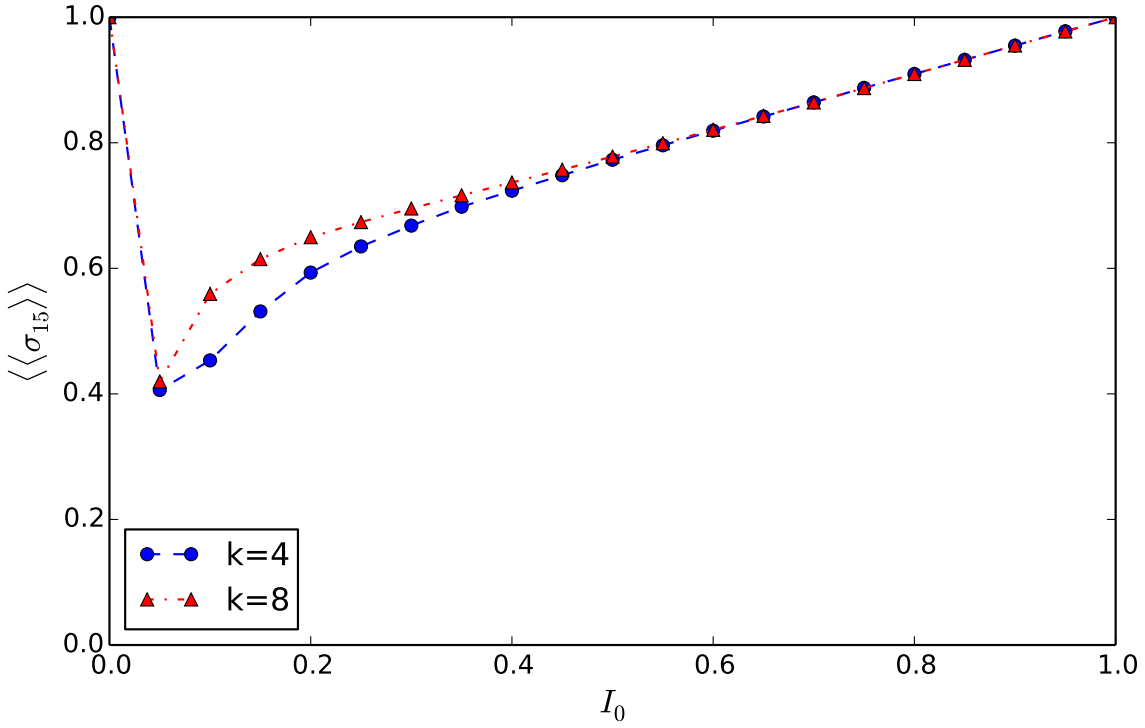

Figure 18: Ensemble averaged transient global synchronization $\langle\langle\sigma_{15}\rangle\rangle$ for different values of I_0, for $K = 4$ and $K = 8$.

We now correlate the ensemble averaged persistent order parameter $\langle\langle I\rangle\rangle$ with $\langle\langle\sigma_{15}\rangle\rangle$ in Fig. 19. *It shows a clear transition from persistence to extinction of the infection as the transient synchrony in the population increses.*

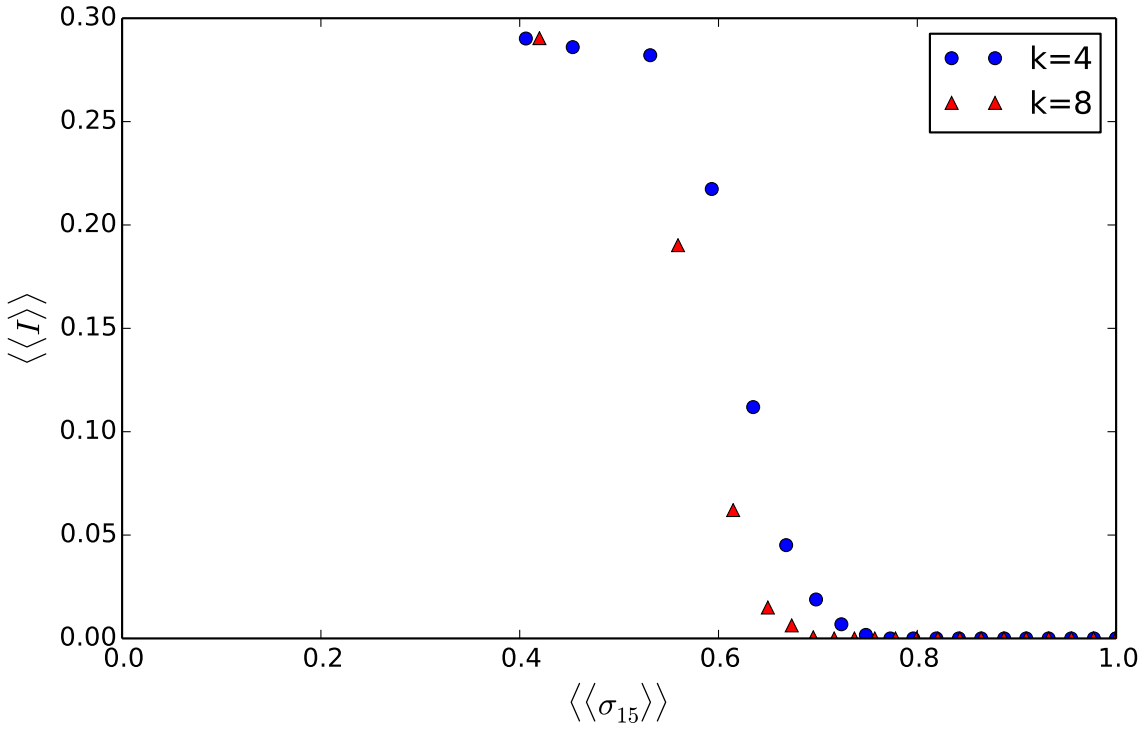

Figure 19: Correlation of the ensemble averaged persistent order parameter $\langle\langle I\rangle\rangle$ with the ensemble and time averaged transient average local synchronization $\langle\langle\sigma_{15}\rangle\rangle$ in the population for $K = 4$ and $K = 8$.

Transient Local Synchronization

We also inquire into the role of transient local synchronization in the population by introducing the transient local synchronization order parameter, given by:

$$\langle \sigma_{L,T} \rangle = \frac{1}{T} \Sigma_{t=0}^{T-1} \sigma_L(t) \tag{10}$$

We also investigate another parameter that quantifies the average root-mean-square deviation in the local synchronization $RMSD(\sigma_L(t))$ during transience, given as:

$$\langle RMSD(\sigma_{L,T}) \rangle = \frac{1}{T} \Sigma_{t=0}^{T-1} RMSD(\sigma_L(t)) \tag{11}$$

where $\sigma_L(t)$ and $RMSD(\sigma_L(t))$ are given by Eqn. 7 and Eqn. 8. Similar to our analysis of the transient global synchronization, we focus on $\langle \sigma_{L,15} \rangle$ and $\langle RMSD(\sigma_{L,15}) \rangle$.

In Fig. 20 below, we look at the correlation between $\langle\langle I\rangle\rangle$ and the ensemble averaged value of the transient average local synchronization $\langle\sigma_{L,15}\rangle$. These values are averaged for 500 random initial conditions for each I_0 for $K = 4$ and $K = 8$. The figure shows a sharp transition in $\langle\langle I\rangle\rangle$, its value being finite only below a certain value of $\langle\sigma_{L,15}\rangle$ for both $K = 4$ and $K = 8$. So it is evident *that some degree of transient local asynchrony is crucial to the survival of the infection in the long run.*

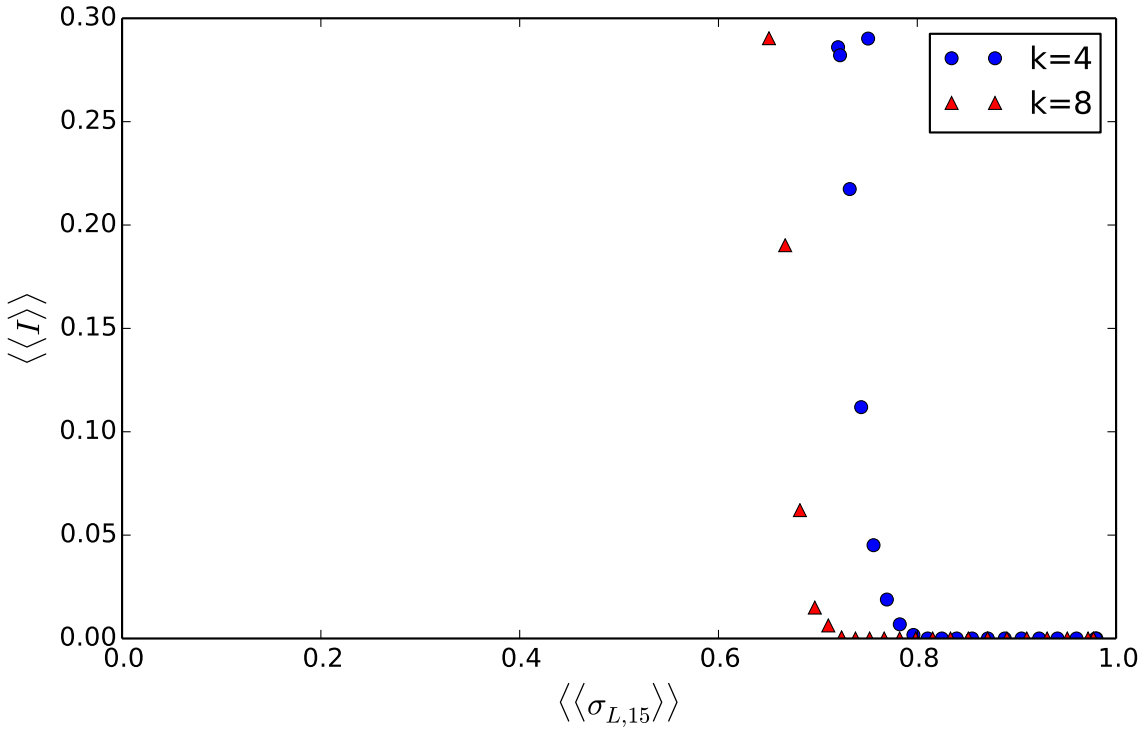

Figure 20: Correlation between the ensemble averaged persistent order parameter $\langle\langle I\rangle\rangle$ and the transient local synchronization order parameter $\langle\langle\sigma_{L,15}\rangle\rangle$ for $K = 4$ and $K = 8$.

We also explore the correlation between $\langle\langle I\rangle\rangle$ and the ensemble averaged value of the root-mean-square deviation in local synchronization during transience. Fig. 21 shows this correlation between $\langle\langle I\rangle\rangle$ and $\langle\langle RMSD(\sigma_{L,15})\rangle\rangle$ obtained for differnt initial fraction of infecteds I_0, where the values are averaged over 500 random initial conditions for each I_0. Again, the figure shows a sharp transition in $\langle\langle I\rangle\rangle$ with an increase in $\langle\langle RMSD(\sigma_{L,15})\rangle\rangle$ depicting that *a significant variance in the synchronization of different neighbourhoods in the population during transience can lead to a higher degree of persistence in the population.*

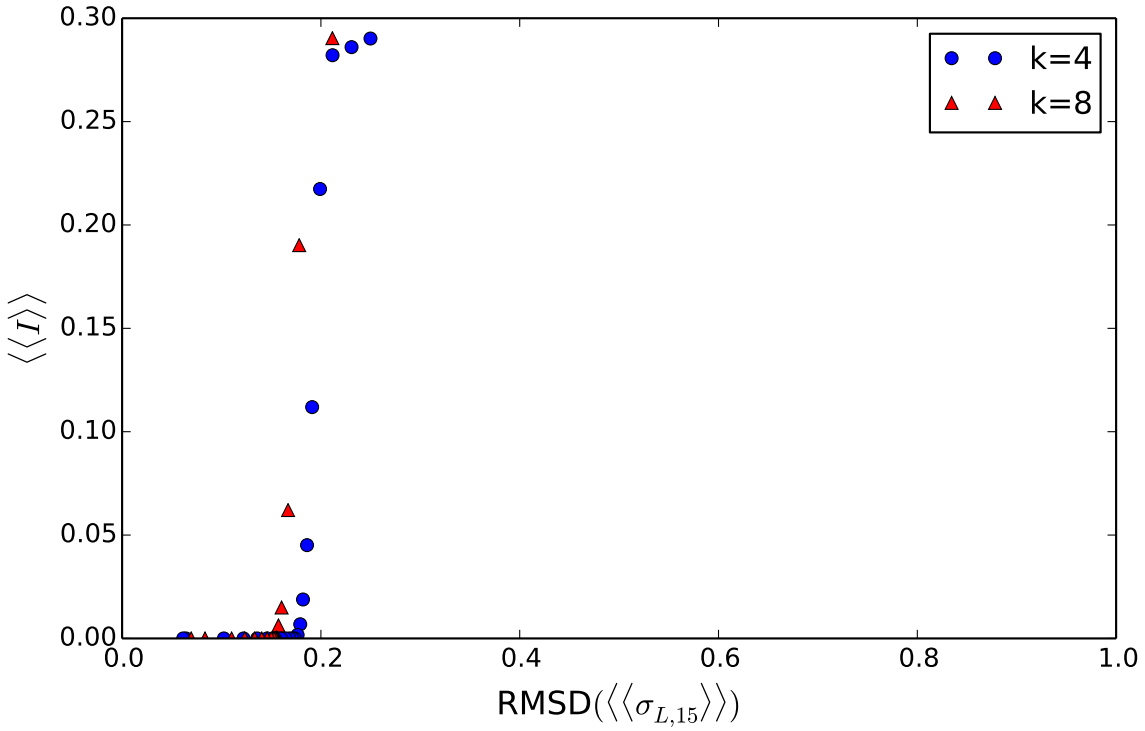

Figure 21: Correlation between the ensemble averaged values of persistent order parameter $\langle\langle I\rangle\rangle$ and the root-mean-square deviation of the local synchronization in the population $\langle\langle RMSD(\sigma_{L,15})\rangle\rangle$ during transience with different initial fraction of infected individuals I_0. The figure shows data for both K= 4 and K = 8.

Discussion

Our analysis of the synchronization in the disease cycle of individuals in a population shows that early asynchrony in the population, both globally and at the local level appear to be a consistent precursor to future persistence of infection. This is an important indication, since it can provide valuable early warning signals for a higher degree of persistence of infectionin a population, thus enabling us to take suitable early action.

Bibliography

[AMS17] Vidit Agrawal, Promit Moitra, and Sudeshna Sinha, *Emergence of persistent infection due to heterogeneity*, Scientific Reports **7** (2017), 41582.

[CH84] Andrew Cliff and Peter Haggett, *Island epidemics*, Scientific American **250** (1984), no. 5, 138147.

[EK88] Leah Edelstein-Keshet, *Mathmetical models in biology*, McGraw-Hill, 1988.

[GCNS02] Michelle Girvan, Duncan S. Callaway, M. E. J. Newman, and Steven H. Strogatz, *Simple model of epidemics with pathogen mutation*, Physical Review E **65** (2002), no. 3.

[GS05] Prashant M. Gade and Sudeshna Sinha, *Dynamic transitions in small world networks: Approach to equilibrium limit*, Physical Review E **72** (2005), no. 5.

[Het76] Herbert W. Hethcote, *Qualitative analyses of communicable disease models*, Mathematical Biosciences **28** (1976), no. 3-4, 335356.

[KA01] Marcelo Kuperman and Guillermo Abramson, *Small world effect in an epidemiological model*, Physical Review Letters **86** (2001), no. 13, 29092912.

[KS13] Vivek Kohar and Sudeshna Sinha, *Emergence of epidemics in rapidly varying networks*, Chaos, Solitons and Fractals **54** (2013), 127134.

[LHS08] A. Litvak-Hinenzon and L. Stone, *Spatio-temporal waves and targeted vaccination in recurrent epidemic network models*, Journal of The Royal Society Interface **6** (2008), no. 38, 749760.

[ML01] Robert M. May and Alun L. Lloyd, *Infection dynamics on scale-free networks*, Physical Review E **64** (2001), no. 6.

[MN00] Cristopher Moore and M. E. J. Newman, *Epidemics and percolation in small-world networks*, Physical Review E **61** (2000), no. 5, 56785682.

[Mur93] J. D. Murray, *Mathematical biology*, Springer-Verlag, 1993.

[RSBY03] Erik M. Rauch, Hiroki Sayama, and Yaneer Bar-Yam, *Dynamics and genealogy of strains in spatially extended hostpathogen models*, Journal of Theoretical Biology **221** (2003), no. 4, 655664.